NeuroImage: Clinical 26 (2020) 102052

Contents lists available at ScienceDirect

NeuroImage: Clinical

journal homepage: www.elsevier.com/locate/ynicl

Longitudinal degradation of the default/salience network axis in symptomatic individuals with elevated amyloid burden.

Aaron P Schultz[a,*], Rachel F Buckley[*,a], Olivia L Hampton[a], Matthew R Scott[a], Michael J Properzi[a], Cleofé Peña-Gómez[c], Jeremy J Pruzin[a,b], Hyun-Sik Yang[b], Keith A Johnson[c], Reisa A Sperling[b], Jasmeer P Chhatwal[a,1]

[a] Harvard Aging Brain Study, Department of Neurology, Massachusetts General Hospital, Harvard Medical School, Boston, MA, United States
[b] Center for Alzheimer Research and Treatment, Department of Neurology, Brigham and Women's Hospital, Harvard Medical School, Boston, Massachusetts, United States
[c] Department of Radiology, Massachusetts General Hospital, Harvard Medical School, Boston, United States

A B S T R A C T

Resting-state functional connectivity MRI (rs-fcMRI) is a non-invasive imaging technique that has come into increasing use to understand disrupted neural network function in neuropsychiatric disease. However, despite extensive study over the past 15 years, the development of rs-fcMRI as a biomarker has been impeded by a lack of reliable longitudinal rs-fcMRI measures. Here we focus on longitudinal change along the Alzheimer's disease (AD) trajectory and demonstrate the utility of Template Based Rotation (TBR) in detecting differential longitudinal rs-fcMRI change between higher and lower amyloid burden individuals with mildly impaired cognition. Specifically, we examine a small ($N = 24$), but densely sampled (~5 observations over ~3 years), cohort of symptomatic individuals with serial rs-fcMRI imaging and PiB-PET imaging for β-amyloid pathology. We observed longitudinal decline of the Default Mode and Salience network axis (DMN/SAL) among impaired individuals with high amyloid burden. No other networks showed differential change in high vs. low amyloid individuals over time. The standardized effect size of AD related DMN/SAL change is comparable to the standardized effect size of amyloid-related change on the mini-mental state exam (MMSE) and hippocampal volume (HV). Last, we show that the AD-related change in DMN/SAL connectivity is almost completely independent of change on MMSE or HV, suggesting that rs-fcMRI is sensitive to an aspect of AD progression that is not captured by these other measures. Together these analyses demonstrate that longitudinal rs-fcMRI using TBR can capture disease-relevant network disruption in a clinical population.

1. Introduction

Network sensitive imaging techniques, especially resting state functional connectivity MRI (rs-fcMRI), have become increasingly important tools to investigate the pathophysiology of neurodegenerative and psychiatric diseases. In the case of Alzheimer's disease (AD), initial reports of decreased default network connectivity in sporadic, late-onset AD (LOAD) have been replicated across a wide spectrum of impairment (Buckner et al., 2009, 2008; Greicius, 2013; Greicius et al., 2003; Hedden et al., 2009; Seeley et al., 2009; Sorg et al., 2007; Sperling et al., 2009; Supekar et al., 2008). In addition to LOAD, decreased default network connectivity has also been well-described in early onset AD (EOAD; (M. Lehmann et al., 2013)) and genetically-driven, autosomal dominant AD (ADAD; (Chhatwal et al., 2018b; J.P. 2013; Thomas et al., 2014). More recent studies that examine multiple networks in the same sample suggest that the degradation of the default network across the spectrum of AD is accompanied by decreased connectivity in a subset of other networks, particularly the salience, dorsal attention, and control networks (Chhatwal et al., 2018b; Thomas et al., 2014), and that the variation in clinical presentation in AD corresponds to variations in networks targeted by the disease process (Lehmann et al., 2015; M. 2013; Ossenkoppele et al., 2015). Importantly, several reports have closely linked connectivity in AD-targeted networks to memory performance (Chhatwal et al., 2018a; Fjell et al., 2016, 2015; Gilmore et al., 2015; Salami et al., 2016; Shaw et al., 2015; Staffaroni et al., 2018; Ward et al., 2014), suggesting that rs-fcMRI may provide an intermediate measure linking AD pathology to cognitive decline.

However, despite relatively consistent findings of altered rs-fcMRI in AD using multiple analytic methods and cohorts, the development of rs-fcMRI metrics as usable biomarkers in clinical and translational research settings has been slowed by difficulties with measurement reliability and longitudinal rs-fcMRI analysis. Owing to a variety of analytic and technical obstacles, reports of longitudinal fcMRI have been fairly few in number, with many focusing on age-related longitudinal change (Fjell et al., 2015; Ng et al., 2016; Persson et al., 2014;

* Corresponding author.
E-mail address: Chhatwal.Jasmeer@mgh.harvard.edu (J.P. Chhatwal).
[1] These authors contributed equally to this work.

https://doi.org/10.1016/j.nicl.2019.102052
Received 2 April 2019; Received in revised form 9 August 2019; Accepted 21 October 2019
Available online 22 October 2019

Salami et al., 2016; Staffaroni et al., 2018). With respect to AD, longitudinal reports of rs-fcMRI changes over time (Deng et al., 2016; Hafkemeijer et al., 2017; Serra et al., 2016; Wang et al., 2012; Zhan et al., 2016) have not specifically assessed how the presence and amount of β-amyloid (Aβ) pathology relate to longitudinal network degradation, an omission which is particularly problematic given that elevated Aβ is one of the defining neuropathologic features of AD. In the present report, we begin to address these issues by leveraging a sample of mildly-impaired older adults followed with longitudinal rs-fcMRI and with available PiBPET to assess fibrillar Aβ burden. This clinically relevant group has been followed closely with longitudinal cognitive measures; Mini Mental State Exam (MMSE) and Clinical Dementia Rating (CDR), as well as structural MRI, allowing us to place rs-fcMRI changes in the context of commonly used clinical measures and imaging biomarkers. This cohort ($N = 24$) has the additional advantage that rs-fcMRI was assessed on a relatively frequent basis during longitudinal follow-up, with the median participant having 5 available rs-fcMRI sessions over approximately 3 years of follow-up.

We utilize template based rotation (TBR) and the network templates derived from (A.P. 2014), in which we have previously demonstrated: cross-sectional relationships between functional connectivity in cognitive networks and cognitive performance (Shaw et al., 2015); an association between baseline rs-fcMRI and longitudinal decline on the preclinical Alzheimer's disease cognitive composite (PACC), particularly in high Aβ individuals (Buckley et al., 2017); AD specific profiles of network disruption (Chhatwal et al., 2018b); cross-sectional relationships to Aβ and tau pathology in cognitively normal elderly (Schultz et al., 2017); and sensitivity to manipulation of the cholinergic system with scopolamine, including a strong relationships between change in rs-fcMRI and subsequent changes to mnemonic memory performance (Chhatwal et al., 2018a). In addition to the standard network descriptions from A.P. Schultz et al. (2014), which include an anti-correlated default mode and salience networks, we also include new template maps for independent default mode and salience networks.

Using this densely-sampled cohort, we test for difference in longitudinal rs-fcMRI change between low and high Aβ subjects. We then compare the fcMRI results to MMSE and hippocampal volume in order to compare the size and independence of the rs-fcMRI effects.

2. Methods

2.1. Participants

24 participants (Female = 6 (25%), age range = 65–83 years) underwent multiple longitudinal structural and resting-state functional MRI (rs-fcMRI) scans, as well as a Pittsburgh compound B positron emission tomography (PIB-PET) scan during the course of the study. All participants completed the Mini-Mental State Examination (MMSE) and the Clinical Dementia Rating scale (CDR). To be included in this study, participants were required to possess at least four rs-fcMRI scans (one completed four scans, twelve completed five scans, three completed six scans, and eight completed seven scans; median = 5 scans) over a period of approximately 3 years. The mean follow-up period was 2.75 years (± 5 months, minimum = 1.6 years, maximum = 3.2 years) for a total of 138 observations across the 24 participants. MRI scans were obtained at baseline, 3-months, 6-months, 12-months, 18-months, 24 months, and 36 months, though resting state fMRI data was not collected at every session. For the sample being used here, we have 15 baseline observations, 20 at 3-months, 16 at 6-months, 24 at 1 year, 23 at 18-months, 19 at 24 months, and 20 at 36 months (see Fig. 1). For subjects without an fcMRI measure at baseline, the zero time was set as the first resting state fMRI scan.

Additionally all 24 participants were required to demonstrate clinically-significant cognitive impairment during the study period. None of the participants were clinically demented at baseline, and met ADNI criteria for MCI at the first instance of CDR 0.5. Accordingly, participants were required to have a baseline global CDR of 0.5 ($N = 22$) or have progressed to a global CDR of 0.5 ($N = 2$) by the end of the study. These 24 subjects were then stratified according to their level of Aβ burden using previously published PiB-PET thresholds (see below). Using this approach, 12 participants were categorized as low-Aβ and 12 as high-Aβ. Six of the subjects were APOE ε4 carriers, 11 were ε4 negative, and 7 did not receive APOE genotyping. Baseline demographics, including breakdowns by Aβ status can be found in Table 1.

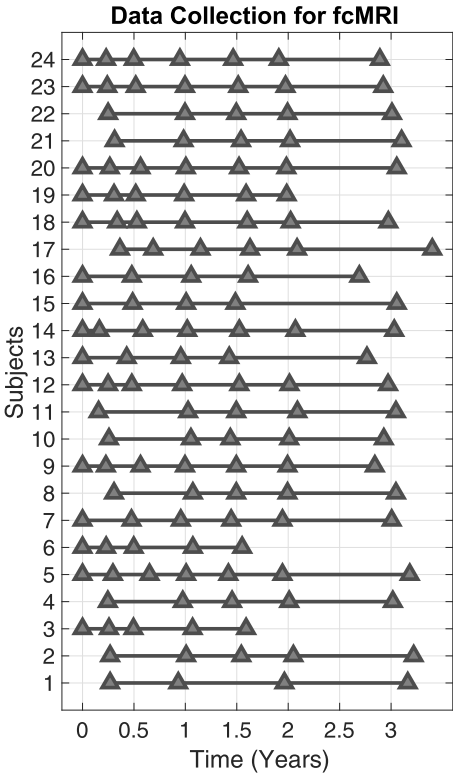

Fig. 1. The timing of fcMRI data collection over a three-year period is shown for each subject.

2.2. Standard protocol approvals, registrations and patient consents

Study protocols were approved by the Partners Healthcare Institutional Review Board, and all participants provided written informed consent prior to the completion of any study procedures.

Table 1
Demographics table showing the whole sample and the sample split by amyloid status. Variables in bold font show a significant difference between low and high amyloid groups, namely low-PiB subjects have an average MMSE score 1.6 points higher, and on average have four months longer follow-up. All non-categorical variables are shown as means ± 1 standard deviation.

	All	Low PiB < 1.186	High Pib > 1.186
N	24	12	12
Age	75.6 ± 5.3	74.0 ± 6.1	77.3 ± 4
Aβ Status	12 low PiB / 12 high PiB	1.04	1.73
Sex	6F / 18M	3F / 9M	3F / 9M
Education(Years)	16.2 ± 2.6	16.2 ± 2.4	16.2 ± 2.8
MMSE	27 ± 2	28.0 ± 1.3	26.4 ± 2.1
Follow up (Years)	2.75 ± 0.43	2.92 ± 0.14	2.57 ± 0.54

2.3. MR imaging

MR images were collected on a 3T Trio Tim scanner (Siemens Medical Systems, Erlangen, Germany) using 12-channel phased-array head coil. Head motion was restrained with extendable foam-padded clamps. Earplugs and noise-reduction headphones were used to attenuate scanner noise.

2.3.1. Structural MRI

Acquisition of structural images consisted of a T1-weighted MPRAGE (160 sagittal slices, with TR = 2.3 s, TE = 2.98 ms, inversion time = 900 ms, flip angle = 9°, FOV = 256 × 240, matrix = 256 × 240, voxel size = 1 × 1 × 1.2 mm). Structural images were processed using FreeSurfer v5.1.

2.3.2. Functional MRI

Functional data were acquired using a gradient-echo-planar pulse sequence (EPI) sensitive to BOLD contrast using the following parameters: TR = 2000 ms, TE = 30 ms, flip angle = 90°, 64 × 64 matrix, FOV = 200 mm, with 3.125 3.125 5 skip 1 mm voxels. Thirty interleaved coronal oblique slices aligned perpendicular to the anterior-posterior commissural plane covered the whole brain. Functional images were acquired in one 6.5 min run of 195 time points at each visit. A cross-hair was projected on a screen at the head of the bore, visible to participants during the scan via a mirror attached to the head coil. Instructions were to lie still, remain awake, and keep eyes open.

All resting state data were processed using SPM12 (http://www.fil.ion.ucl.ac.uk/spm/). Each run was slice-time corrected, followed by a single realignment and coregistration across all timepoints, where each volume was realigned to the first volume of each run, then realigned to the first session. This was followed by a second pass realignment to the mean EPI image across all sessions. The mean-across-time EPI image was then directly normalized to MNI space using the SPM12 unified segmentation and normalization routine (Calhoun et al., 2017) and then applied to the data. Spatial normalization to template space was followed by spatial smoothing with a 6 mm FWHM Gaussian kernel, followed by removal of temporal frequencies below 0.08 Hz, and temporal z-scoring of each time course.

Functional connectivity measurements were made using Template Based Rotation (TBR (A.P. Schultz et al., 2014)). Briefly, TBR works by mapping variance from a given subject's fMRI run to a set of *a priori* template maps. Template maps are derived from a large outside sample. The process produces a least squares fit to the template maps via a weighted linear summation of functional volumes. The weights associated with each functional volume can be interpreted as a time series that best recapitulates the spatial pattern in the templates. Full details can be found in A.P. Schultz et al. (2014).

Measures were derived for the following cognitive networks: Default Mode (DMN) / Salience (SAL), Dorsal Attention (DAN), Frontoparietal Control (Left/Right FPCN), and the Motor network using the network templates from A.P. Schultz et. al. (2014). Having the DMN and SAL in a single component means that both networks are represented with a single variance component that is positively correlated with DMN regions and negatively correlated with SAL regions. This, however, leaves open the possibility of variance components that are shared across DMN regions and orthogonal to SAL regions and vice versa. To address this issue, we also included two additional components (Fig. 2) derived using the same data and methods, except without row-based normalization. This resulted in separate components for the DMN and SAL (see A.P. Schultz et al. (2014) for details about row-based normalization and the derivation of the template maps). Fig. 2 shows the separate DMN and SAL templates as well as the combined DMN/SAL template used for the main analyses. The addition of these two additional templates allows us to more directly assess differences between DMN and SAL networks relative to a unitary DMN/SAL network axis. Detailed depictions of the other template maps can be found in (A.P. Schultz et al., 2014 and Chhatwal et al., 2018). Template maps and relevant code for TBR are publicly available at mrtools.mgh.harvard.edu. TBR connectivity measures for each session and each network were calculated by using a spatial correlation to compute the similarity of the connectivity map from each fcMRI session to the template map. One time-point from one subject was dropped due to abnormally low connectivity measures, both with respect to the subject and with respect to the sample as a whole. Manual inspection of the scan revealed notable spatial artifacts.

As with spatial group independent component analysis (ICA), when using TBR there is no explicit requirement to clean data (Power et al., 2014) (e.g. motion correction, data scrubbing, nuisance regression) in advance of analysis (A.P. Schultz et al., 2014). ICA can be written in matrix algebra as IC = X•M where IC is the independent components (m-voxels by n-components), M is the unmixing matrix (m-volumes by n-components), and X is the empirical data (m-voxels by n-volumes). Starting with only X, M must be discovered which then provides IC. If IC is already known, then the derivation of M is a straightforward algebraic problem that can be solved as $M = X^{-1}$•IC, which is precisely the TBR formulation (where X^{-1} is the pseudo-inverse of the matrix X). The only assumption is that a given IC, derived on an independent dataset, is a sufficiently close approximation to a true source in X, and is independent of nuisance variance sources. This provides TBR with an implicit ability to perform blind source/signal separation even when not explicitly modeling all sources. Additionally, prior work strongly suggests that nearly all approaches to cleaning fMRI data result in lower measurement reliability (Shirer et al., 2015), a potentially critical problem in longitudinal analyses. Given the focus here on longitudinal change in fcMRI measures and the inherent source/signal separability of TBR, we minimized data cleaning as much as possible to avoid diminished measurement reliability as a source of spurious within-subject variability across time.

2.4. PET imaging

Acquisition of ^{11}C Pittsburgh Compound B PET data has previously been described in detail (Becker et al., 2011; Johnson et al., 2007; Sperling et al., 2009). In brief, PiB PET images were acquired with an 8.5 to 15 mCi bolus injection followed by a 60-minute dynamic acquisition in 69 vol (12 × 15 s, 57 × 60 s). PET data were reconstructed, attenuation corrected, scatter corrected, and evaluated for excessive head motion. Data from the first 8 min post injection was used to co-register the data to the T1 image for each subject using a 6 DoF rigid body registration. A summary distribution volume ratio (DVR) computed with Logan plotting was derived from a target region composed of frontal, lateral and retrosplenial tracer uptake (FLR) and a cerebellar grey reference region. The regions comprising the FLR are known to show elevated PiB binding in AD dementia patients (8). The cutoff of PiB FLR DVR > 1.186 for Aβ positivity was derived on a reference sample using Gaussian mixture modeling as previously described (Mormino et al., 2014a; E.C. 2014b).

2.5. Clinical measures

The MMSE (Folstein et al., 1975) and CDR (Morris, 1993) were obtained annually at baseline, 12-months, 24 months, and 36 months. Due to missing observations relative the MRI acquisitions, intermediate measures for MMSE were temporally imputed to align with MRI data. Within subject temporal imputation utilized resampling with a shape preserving piecewise cubic spline interpolation.

2.6. Analyses

Analyses were performed using linear mixed effects (LME) models using the *fitlme* routine in the MATLAB 2018b statistics package using default settings. Subject level random effects for both intercept

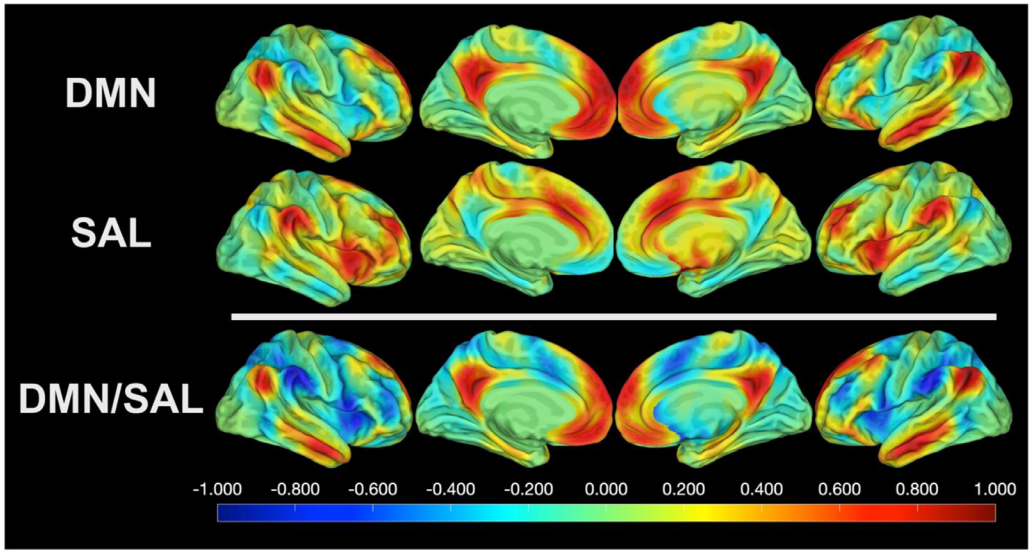

Fig. 2. To assess rs-fcMRI in DMN and SAL independently, we generated an alternate template set by omitting row-based normalization. This approach yielded separate maps for the DMN and SAL. The top row shows a surface projection of the independent DMN components. The middle row shows a surface projection of the independent SAL component. The third row shows the combined DMN/SAL template from A.P. Schultz et al., 2014.

(subject) and slope (time) were included in all LME models. Models were constructed to ascertain the relationship of baseline Aβ to longitudinal change in rs-fcMRI networks. The primary effect of interest was the PiB•time interaction term. We chose to use PiB-PET as a continuous measure rather than dichotomizing, and time was based on the dates of the MRI acquisitions with 0-time set as the first rs-fcMRI scan. To control for spurious and confounding effects we included between-subjects covariates for age, sex, and years of education, including interactions with time. We also included time-varying estimates of subject motion, time-varying cortical gray matter volume, and time-varying intracranial volume to correct for variability in the FreeSurfer recons, gross differences in head size, and cortical atrophy. Subject motion was computed as the average framewise displacement across the functional run. To achieve this we computed the Euclidean distance between the origin of each frame as estimated by the realignment procedure, and then computed the average distance moved between frames. Due to between subject distributions of motion tending towards positive skew, these measures were log-transformed to generate normal distributions.

Our dependent variables included multiple fcMRI networks including the default mode with anti-correlated salience network (DMN/SAL), DMN, SAL, the dorsal attention (DAN), left and right frontoparietal control networks (rFPCN and lFPCN), primary visual (VIS), and motor (MOT) networks. To help contextualize the results, and to investigate whether fcMRI signal was capturing a unique channel of information, we also performed analyses using longitudinal hippocampal volume (HV), and longitudinal MMSE. Raw data plots (as a function of age) depicting the data being modeled are shown in Fig. 3 for the DMN/SAL (Fig. 3A), DMN (Fig. 3B), MMSE (Fig. 3C), and HV (Fig. 3D).

3. Results

3.1. Effect of Aβ on longitudinal change in fcMRI network strength

The only network to show a significant PiB•Time effect was the DMN/SAL network where we observed that higher PiB-PET signal is associated with a greater rate of decline in DMN/SAL network coherence ($t(125) = -3.15$ $p = 0.002$; Fig. 5A), indicating that the DMN and SAL networks are becoming less coordinated and more orthogonal. Left and Right FPCN both showed trend level effects (lFPCN: $t(125) = -1.89$, $p = 0.063$. rFPCN: $t(125) = -1.65$, $p = 0.102$). Neither the DMN alone ($t(125) = -1.02$ $p = 0.310$; Fig. 5B) nor SAL alone ($t(125) = -1.25$, $p = 0.213$) showed a significant effect on their own, suggesting that incorporating the strength of inter-network connections between the DMN and SAL improves the ability to detect change along an AD trajectory. Standardized β estimates with error bars for all dependent variables are shown in Fig. 4.

3.2. Effect of Aβ on longitudinal change on MMSE and Hippocampal Volume

To contextualize the size of the DMN/SAL effect, we also ran the same model using an established AD clinical measure, the MMSE, and an established imaging marker of AD neurodegeneration, hippocampal volume (Fig. 4). The MMSE showed a significant PiB•Time effect ($t(125) = -2.56$, $p = 0.012$; Fig. 5C), as did hippocampal volume ($t(125) = -3.49$, $p < 0.001$; Fig. 5D). These values correspond to a Cohen's D of 0.56 for DMN/SAL, 0.46 for MMSE, and 0.62 for hippocampal volume, where 0.2 is considered a small effect, 0.5 a medium effect, and 0.8 a large effect.

3.3. Does longitudinal variance in DMN/SAL fcMRI overlap with MMSE or HV?

To address this question we re-ran the longitudinal LME from above with DMN/SAL fcMRI as the dependent variable and then added time-varying MMSE and HV as covariates in the model. The PiB•Time effect on longitudinal DMN/SAL fcMRI remained largely unchanged ($t(123) = -2.98$, $p = 0.003$, $D = 0.53$), and we did not observe significant relationships with either MMSE ($t(123) = 0.42$, $p = 0.672$) or HV ($t(123) = -0.70$, $p = 0.483$), indicating the DMN/SAL fcMRI metric captures an aspect of disease progression not represented in these commonly used measures of cognition and neurodegeneration.

3.4. Effects on DMN/SAL fcMRI with reduced covariates

Due to concerns with nuisance variance and confounding factors we took a conservative approach to controlling for potentially confounding sources of variance. The models utilized here included time-varying motion, time varying cortical volume, and time varying intracranial volume. Additionally, we controlled for between subject variance in age, sex, and education (including interactions with time). As such we also wanted to report results from the simplified model: DMN ~ PiB•Time + (Time|Subject). As expected without the additional covariates the PiB•Time effect was more robust ($t(134) = 4.02$, $p < 0.001$, $D = 0.69$).

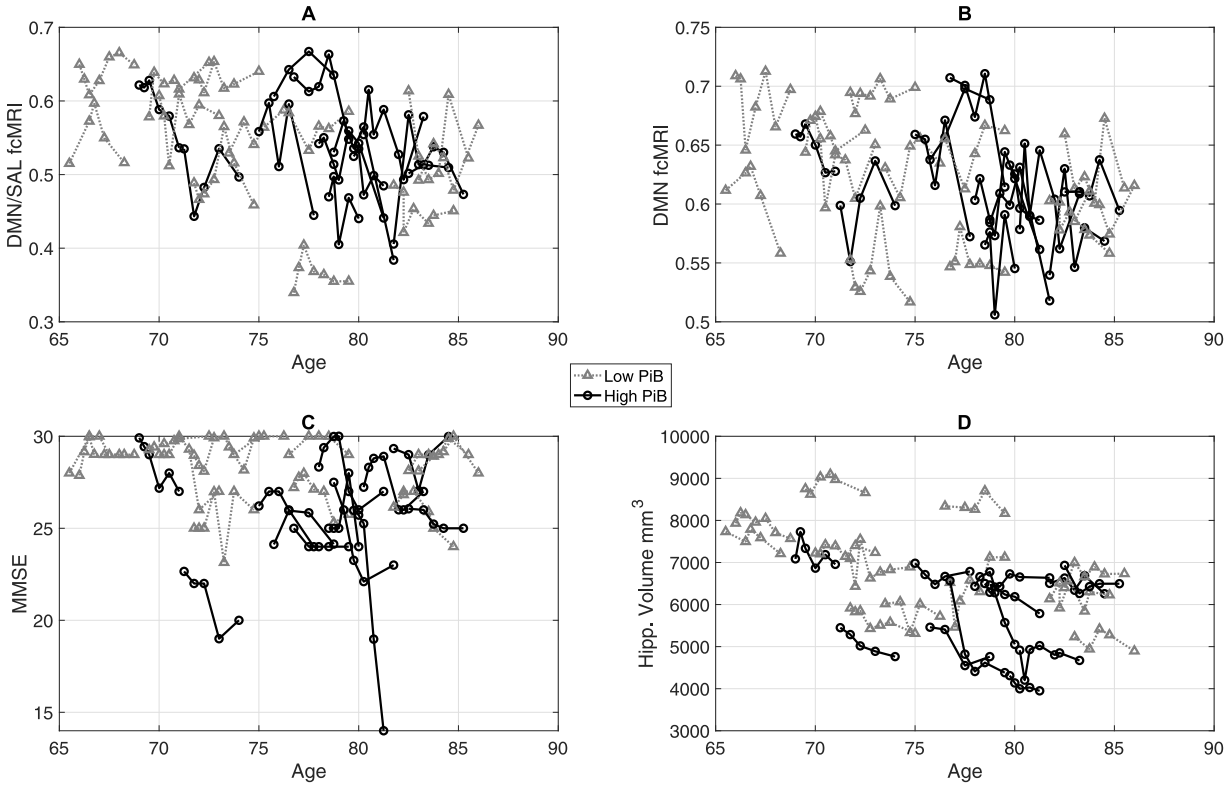

Fig. 3. Depiction of raw longitudinal data by age. Each subject is depicted with a single line. Low-PiB subjects are shown in grey with triangle markers. High-PiB subjects are shown in black with circular markers. Panel A (upper-left) shows the raw longitudinal data for the DMN/SAL network component which showed a significant PiB•Time effect. Panel B shows the independent DMN component which did not show a significant PiB•Time effect. Panel C shows the longitudinal data for the MMSE, and Panel D shows the longitudinal data for Hippocampal Volume.

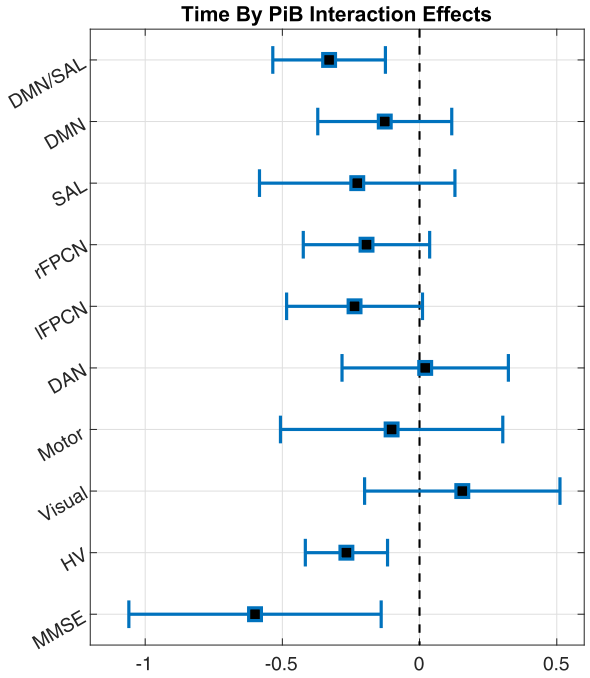

Fig. 4. Standardized beta coefficients with 95% confidence intervals for the PiB•time effect. Each measure was used individually as a dependent variable in a longitudinal LME model assessing the effects of amyloid burden over time. Only DMN/SAL, HV, and MMSE showed significant effects ($p < 0.05$), though the left and right FPCN were observed as trend level effects. All significant effects survived multiple comparison correction.

4. Discussion

We observed that progressive degradation of the coordinated Default-Salience network axis over a three-year period distinguished high from low Aβ clinically impaired individuals during longitudinal follow-up. Further, we observed that DMN/SAL network measurements which incorporate both within and between network connectivity were superior to measures that only assessed within-network change in the DMN or SAL. No other network showed a significant relationship between Aβ burden and longitudinal change of functional connectivity. The effect of Aβ burden on longitudinal change of DMN/SAL network coherence was similar in effect size to change in hippocampal volume and MMSE, and the DMN/SAL effect was nearly fully independent of change on both the MMSE and hippocampal volume. This suggests that DMN/SAL rs-fcMRI is capturing a unique channel of information regarding AD progression that is not reflected in hippocampal volume or MMSE.

Of the prior reports on longitudinal rs-fcMRI, our results are most comparable with Zhan et al., 2016, where inter-network correlation between the DMN and SAL was disrupted, particularly in the early MCI cohort. The significant PiB•Time effect for the DMN/SAL is also consistent with prior reports using this DMN/SAL network template (Buckley et al., 2017; Chhatwal et al., 2018a, 2018b; Schultz et al., 2017; A.P. 2014; Shaw et al., 2015). However, with the exception of Schultz et al., 2017 (where relationships with markers of AD molecular pathology were limited to the DMN and SAL), these other reports all found significant effects with other networks in addition to the DMN/SAL, especially the Left/Right FPCN. Perhaps owing to sample size, significant findings in the present report were only observed with respect to the DMN/SAL axis, with FPCN changes at a trend-level. It remains to be seen whether the DMN/SAL effect is particular to the AD pathological cascade or if it is simply a consequence of more stable

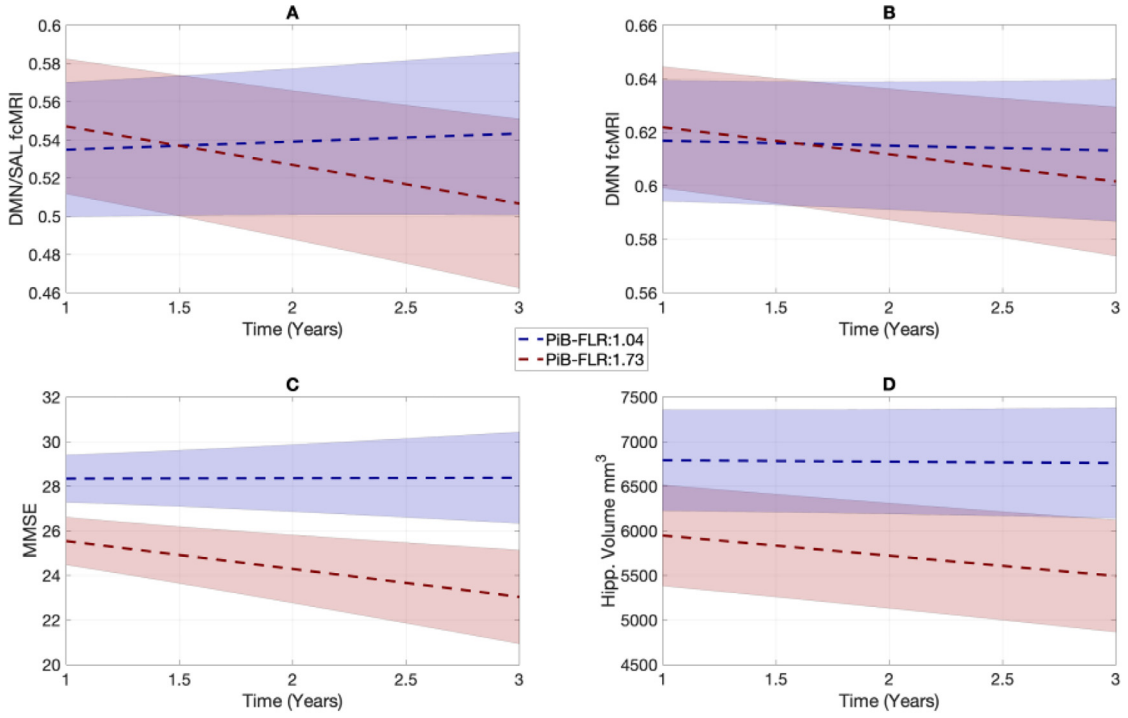

Fig. 5. Unadjusted plots of model fits for change over time across four different variables. Panel A shows the LME model fits for DMN/SAL connectivity over time showing greater decline over time in high PiB as compare to low PiB subjects. Panel B shows similar slopes between low/high PiB groups for the independent DMN component. C shows greater decline of MMSE over time in the high-PiB group. Panel D shows greater decline in hippocampal volume over time in high-PiB subjects as compared to low-PIB subjects.

longitudinal measures or modestly increased power relative to other network measures.

Though more work is needed to further develop maximally sensitive connectivity metrics, these results are promising for fcMRI as a longitudinal marker. This is especially intriguing given that many current and upcoming clinical trials are collecting resting state fMRI data for use as an exploratory secondary outcome measure, providing fertile ground for further development of fcMRI as an AD biomarker.

The results presented are best understood in the context of several important limitations. First, these results are from an early symptomatic cohort; it remains to be seen whether these results will translate to earlier preclinical stages of Alzheimer's disease. Second the sample size is relatively small, consisting of 24 subjects. Accordingly, the observed effect sizes should be interpreted with caution and replication in other samples will be important to confirm these results. It should also be noted the small sample size is compensated by an average of 5 observations over approximately three years. This dense sampling makes this a unique cohort relative to most currently published reports on longitudinal functional connectivity. Third, prior work strongly suggests that tau pathologic burden may be more tightly correlated with cognitive impairment as compared to Aβ burden. The lack of tau-PET imaging in the sample studied here leaves open several questions regarding the link between tau pathology and change in the DMN/SAL fcMRI that will need to be addressed in future studies.

We find these results encouraging for the use of fcMRI as a longitudinal measure of Aβ related pathological change. While rs-fcMRI is not without flaws, it remains a powerful technique for observing and measuring brain function *in-vivo*, provides a good balance of spatial and temporal resolution, uses no ionizing radiation, and is relatively low cost. This is especially true in the context of clinical trials where MRI is needed for safety monitoring, and structural MRI is used for processing of other modalities such as PET imaging. The addition of rs-fcMRI adds very little additional subject burden and is being acquired in many current and upcoming clinical trials. Although rs-fcMRI has shown promise as a functional brain measure, it has yet to fulfill its potential as a clinically useful measure for AD and other neurodegenerative diseases. This is largely due to relatively poor measurement reliability which is a product of both the high degree of dynamicity inherent to fMRI, coupled with multiple sources of nuisance variance and measurement noise. Our findings support the further development of rs-fcMRI as an AD biomarker and, more broadly, suggests that rs-fcMRI may be usable as an exploratory outcome measure in neuropsychiatric disease clinical and translational research.

Acknowledgements

This research was supported grant funding from the National Institute on Aging at the National Institute of Health (NIA-NIH) primarily via R01AG027435, and in addition to the Harvard Aging Brain Study (P01AG036694), as well as R21AG060221, K23AG049087, K99AG061238, and K24AG035007.

This research was carried out at the Athinoula A. Martinos Center for Biomedical Imaging at the Massachusetts General Hospital, using resources provided by the Center for Functional Neuroimaging Technologies [P41EB015896], a P41 Biotechnology Resource Grant supported by the National Institute of Biomedical Imaging and Bioengineering (NIBIB), National Institutes of Health. This work also involved the use of instrumentation supported by the NIH Shared Instrumentation Grant Program and/or High-End Instrumentation Grant Program; specifically S10RR021110, S10RR023401, S10RR019307, S10RR019254, and S10RR023043.

Reference

Becker, J.A., Hedden, T., Carmasin, J., Maye, J., Rentz, D.M., Putcha, D., Fischl, B., Greve, D.N., Marshall, G.A., Salloway, S., 2011. Amyloid-β associated cortical thinning in clinically normal elderly. Ann. Neurol. 69, 1032–1042.

Buckley, R.F., Schultz, A.P., Hedden, T., Papp, K.V., Hanseeuw, B.J., Marshall, G., Sepulcre, J., Smith, E.E., Rentz, D.M., Johnson, K.A., Sperling, R.A., Chhatwal, J.P., 2017. Functional network integrity presages cognitive decline in preclinical

Alzheimer disease. Neurology 89, 29–37.
Buckner, R.L., Andrews-Hanna, J.R., Schacter, D.L., 2008. The brain's default network: anatomy, function, and relevance to disease. Ann. N. Y. Acad. Sci. 1124, 1–38.
Buckner, R.L., Sepulcre, J., Talukdar, T., Krienen, F.M., Liu, H., Hedden, T., Andrews-Hanna, J.R., Sperling, R.A., Johnson, K.A., 2009. Cortical hubs revealed by intrinsic functional connectivity: mapping, assessment of stability, and relation to alzheimer's disease. Journal of Neuroscience 29, 1860–1873.
Calhoun, V.D., Wager, T.D., Krishnan, A., Rosch, K.S., Seymour, K.E., Nebel, M.B., Mostofsky, S.H., Nyalakanai, P., Kiehl, K., 2017. The impact of T1 versus epi spatial normalization templates for fMRI data analyses. Hum. Brain Mapp. 20, 812–870.
Chhatwal, J.P., Schultz, A.P., Hedden, T., Boot, B.P., Wigman, S., Rentz, D., Johnson, K.A., Sperling, R.A., 2018a. Anticholinergic amnesia is mediated by alterations in human network connectivity architecture. Cereb. Cortex. https://doi.org/10.1093/cercor/bhy214.
Chhatwal, J.P., Schultz, A.P., Johnson, K.A., Hedden, T., Jaimes, S., Benzinger, T.L.S., Jack, C., Jr, Ances, B.M., Ringman, J.M., Marcus, D.S., Ghetti, B., Farlow, M.R., Danek, A., Levin, J., Yakushev, I., Laske, C., Koeppe, R.A., Galasko, D.R., Xiong, C., Masters, C.L., Schofield, P.R., Kinnunen, K.M., Salloway, S., Martins, R.N., McDade, E., Cairns, N.J., Buckles, V.D., Morris, J.C., Bateman, R., Sperling, R.A., Dominantly Inherited Alzheimer Network, 2018b. Preferential degradation of cognitive networks differentiates alzheimer's disease from ageing. Brain. https://doi.org/10.1093/brain/awy053.
Chhatwal, J.P., Schultz, A.P., Johnson, K., Benzinger, T.L.S., Jack, C., Jr, Ances, B.M., Sullivan, C.A., Salloway, S.P., Ringman, J.M., Koeppe, R.A., Marcus, D.S., Thompson, P., Saykin, A.J., Correia, S., Schofield, P.R., Rowe, C.C., Fox, N.C., Brickman, A.M., Mayeux, R., McDade, E., Bateman, R., Fagan, A.M., Goate, A.M., Xiong, C., Buckles, V.D., Morris, J.C., Sperling, R.A., 2013. Impaired default network functional connectivity in autosomal dominant alzheimer disease. Neurology 81, 736–744.
Deng, Y., Liu, K., Shi, L., Lei, Y., Liang, P., Li, K., Chu, W.C.W., Wang, D., Initiative, Alzheimer's Disease Neuroimaging, 2016. Identifying the alteration patterns of brain functional connectivity in progressive mild cognitive impairment patients: a longitudinal whole-brain voxel-wise degree analysis. Front. Aging Neurosci. 8, 195.
Fjell, A.M., Sneve, M.H., Grydeland, H., Storsve, A.B., de Lange, A.-M.G., Amlien, I.K., Røgeberg, O.J., Walhovd, K.B., 2015. Functional connectivity change across multiple cortical networks relates to episodic memory changes in aging. Neurobiol. Aging 36, 3255–3268.
Fjell, A.M., Sneve, M.H., Storsve, A.B., Grydeland, H., Yendiki, A., Walhovd, K.B., 2016. Brain events underlying episodic memory changes in aging: a longitudinal investigation of structural and functional connectivity. Cereb. Cortex 26, 1272–1286.
Folstein, M.F., Folstein, S.E., McHugh, P.R., 1975. “Mini-mental state”. a practical method for grading the cognitive state of patients for the clinician. J. Psychiatr. Res 12, 189–198.
Gilmore, A.W., Nelson, S.M., McDermott, K.B., 2015. A parietal memory network revealed by multiple mri methods. Trends Cogn. Sci. 19, 534–543.
Greicius, M., 2013. Network-based neurodegeneration in alzheimer's disease: evidence from resting-state fMRI. Alzheimers. Dement. 9, P313.
Greicius, M.D., Krasnow, B., Reiss, A.L., Menon, V., 2003. Functional connectivity in the resting brain: a network analysis of the default mode hypothesis. Proceedings of the National Academy of Sciences 100, 253–258.
Hafkemeijer, A., Möller, C., Dopper, E.G.P., Jiskoot, L.C., van den Berg-Huysmans, A.A., van Swieten, J.C., van der Flier, W.M., Vrenken, H., Pijnenburg, Y.A.L., Barkhof, F., Scheltens, P., van der Grond, J., Rombouts, S.A.R.B., 2017. A longitudinal study on resting state functional connectivity in behavioral variant frontotemporal dementia and alzheimer's disease. J. Alzheimers. Dis. 55, 521–537.
Hedden, T., Van Dijk, K.R.A., Alex Becker, J., Mehta, A., Sperling, R.A., Johnson, K.A., Buckner, R.L., 2009. Disruption of functional connectivity in clinically normal older adults harboring amyloid burden. J. Neurosci. 29, 12686–12694.
Johnson, K.A., Gregas, M., Becker, J.A., Kinnecom, C., Salat, D.H., Moran, E.K., Smith, E.E., Rosand, J., Rentz, D.M., Klunk, W.E., Mathis, C.A., Price, J.C., Dekosky, S.T., Fischman, A.J., Greenberg, S.M., 2007. Imaging of amyloid burden and distribution in cerebral amyloid angiopathy. Ann. Neurol. 62, 229–234.
Lehmann, M., Madison, C., Ghosh, P.M., Miller, Z.A., Greicius, M.D., Kramer, J.H., Coppola, G., Miller, B.L., Jagust, W.J., Gorno-Tempini, M.L., Seeley, W.W., Rabinovici, G.D., 2015. Loss of functional connectivity is greater outside the default mode network in nonfamilial early-onset alzheimer's disease variants. Neurobiol. Aging 36, 2678–2686.
Lehmann, M., Madison, C.M., Ghosh, P.M., Seeley, W.W., Mormino, E., Greicius, M.D., Gorno-Tempini, M.L., Kramer, J.H., Miller, B.L., Jagust, W.J., Rabinovici, G.D., 2013. Intrinsic connectivity networks in healthy subjects explain clinical variability in alzheimer's disease. Proc. Natl. Acad. Sci. U. S. A. 110, 11606–11611.
Mormino, E.C., Betensky, R.A., Hedden, T., Schultz, A.P., Amariglio, R.E., Rentz, D.M., Johnson, K.A., Sperling, R.A., 2014a. Synergistic effect of β-amyloid and neurodegeneration on cognitive decline in clinically normal individuals. JAMA Neurol 71, 1379–1385.
Mormino, E.C., Betensky, R.A., Hedden, T., Schultz, A.P., Ward, A., Huijbers, W., Rentz, D.M., Johnson, K.A., Sperling, R.A., 2014b. Alzheimer's disease neuroimaging initiative, australian imaging biomarkers and lifestyle flagship study of ageing. Harvard Aging Brain Study 82, 1760–1767 Amyloid and APOE ε4 interact to influence short-term decline in preclinical Alzheimer disease. Neurology.
Morris, J.C., 1993. The clinical dementia rating (CDR): current version and scoring rules. Neurology 43, 2412–2414.
Ng, K.K., Lo, J.C., Lim, J.K.W., Chee, M.W.L., Zhou, J., 2016. Reduced functional segregation between the default mode network and the executive control network in healthy older adults: a longitudinal study. Neuroimage 133, 321–330.
Ossenkoppele, R., Cohn-Sheehy, B.I., La Joie, R., Vogel, J.W., M??ller, C., Lehmann, M., Van Berckel, B.N.M., Seeley, W.W., Pijnenburg, Y.A., Gorno-Tempini, M.L., Kramer, J.H., Barkhof, F., Rosen, H.J., Van der Flier, W.M., Jagust, W.J., Miller, B.L., Scheltens, P., Rabinovici, G.D., 2015. Atrophy patterns in early clinical stages across distinct phenotypes of alzheimer's disease. Hum. Brain Mapp. 36, 4421–4437.
Persson, J., Pudas, S., Nilsson, L.-.G., Nyberg, L., 2014. Longitudinal assessment of default-mode brain function in aging. Neurobiol. Aging 35, 2107–2117.
Power, J.D., Mitra, A., Laumann, T.O., Snyder, A.Z., Schlaggar, B.L., Petersen, S.E., 2014. Methods to detect, characterize, and remove motion artifact in resting state fMRI. Neuroimage 84, 320–341.
Salami, A., Wåhlin, A., Kaboodvand, N., Lundquist, A., Nyberg, L., 2016. Longitudinal evidence for dissociation of anterior and posterior mtl resting-state connectivity in aging: links to perfusion and memory. Cereb. Cortex 26, 3953–3963.
Schultz, A.P., Chhatwal, J.P., Hedden, T., Mormino, E.C., Hanseeuw, B.J., Sepulcre, J., Huijbers, W., LaPoint, M., Buckley, R.F., Johnson, K.A., Sperling, R.A., 2017. Phases of hyperconnectivity and hypoconnectivity in the default mode and salience networks track with amyloid and tau in clinically normal individuals. J. Neurosci. 37, 4323–4331.
Schultz, A.P., Chhatwal, J.P., Huijbers, W., Hedden, T., Van Dijk, K.R.A., McLaren, D.G., Ward, A.M., Wigman, S.E., Sperling, R.A., 2014. Template based rotation: a method for functional connectivity analysis with a priori templates. Neuroimage 102 (Pt 2), 620–636.
Seeley, W.W., Crawford, R.K., Zhou, J., Miller, B.L., Greicius, M.D., 2009. Neurodegenerative diseases target large-scale human brain networks. Neuron 62, 42–52.
Serra, L., Cercignani, M., Mastropasqua, C., Torso, M., Spanò, B., Makovac, E., Viola, V., Giulietti, G., Marra, C., Caltagirone, C., Bozzali, M., 2016. Longitudinal changes in functional brain connectivity predicts conversion to alzheimer's disease. J. Alzheimers. Dis. 51, 377–389.
Shaw, E.E., Schultz, A.P., Sperling, R.A., Hedden, T., 2015. Functional connectivity in multiple cortical networks is associated with performance across cognitive domains in older adults. Brain Connect 5, 505–516.
Shirer, W.R., Jiang, H., Price, C.M., Ng, B., Greicius, M.D., 2015. Optimization of rs-fMRI pre-processing for enhanced signal-noise separation, test-retest reliability, and group discrimination. Neuroimage 117, 67–79.
Sorg, C., Riedl, V., Mühlau, M., Calhoun, V.D., Eichele, T., Läer, L., Drzezga, A., Förstl, H., Kurz, A., Zimmer, C., Wohlschläger, A.M., 2007. Selective changes of resting-state networks in individuals at risk for Alzheimer's disease. Proceedings of the National Academy of Sciences 104, 18760–18765.
Sperling, R.A., Laviolette, P.S., O'Keefe, K., O'Brien, J., Rentz, D.M., Pihlajamaki, M., Marshall, G., Hyman, B.T., Selkoe, D.J., Hedden, T., Buckner, R.L., Becker, J.A., Johnson, K.A., 2009. Amyloid deposition is associated with impaired default network function in older persons without dementia. Neuron 63, 178–188.
Staffaroni, A.M., Brown, J.A., Casaletto, K.B., Elahi, F.M., Deng, J., Neuhaus, J., Cobigo, Y., Mumford, P.S., Walters, S., Saloner, R., Karydas, A., Coppola, G., Rosen, H.J., Miller, B.L., Seeley, W.W., Kramer, J.H., 2018. The longitudinal trajectory of default mode network connectivity in healthy older adults varies as a function of age and is associated with changes in episodic memory and processing speed. J. Neurosci. 38, 2809–2817.
Supekar, K., Menon, V., Rubin, D., Musen, M., Greicius, M.D., 2008. Network analysis of intrinsic functional brain connectivity in alzheimer's disease. PLoS Comput. Biol. 4, e1000100.
Thomas, J.B., Brier, M.R., Bateman, R.J., Snyder, A.Z., Benzinger, T.L., Xiong, C., Raichle, M., Holtzman, D.M., Sperling, R.A., Mayeux, R., Ghetti, B., Ringman, J.M., Salloway, S.A., McDade, E., Rossor, M.N., Ourselin, S., Schofield, P.R., Masters, C.L., Martins, R.N., Weiner, M.W., Thompson, P.M., Fox, N.C., Koeppe, R.A., Jack, C.R., Jr, Mathis, C.A., Oliver, A., Blazey, T.M., Moulder, K., Buckles, V., Hornbeck, R., Chhatwal, J.P., Schultz, A.P., Goate, A.M., Fagan, A.M., Cairns, N.J., Marcus, D.S., Morris, J.C., Ances, B.M., 2014. Functional connectivity in autosomal dominant and late-onset alzheimer disease. JAMA Neurol 71, 1111–1122.
Wang, Z., Liang, P., Jia, X., Jin, G., Song, H., Han, Y., Lu, J., Li, K., 2012. The baseline and longitudinal changes of pcc connectivity in mild cognitive impairment: a combined structure and resting-state fMRI study. PLoS ONE 7, e36838.
Ward, A.M., Schultz, A.P., Huijbers, W., Dijk, K., 2014. The parahippocampal gyrus links the default-mode cortical network with the medial temporal lobe memory system. Hum. Brain Mapp.
Zhan, Y., Ma, J., Alexander-Bloch, A.F., Xu, K., Cui, Y., Feng, Q., Jiang, T., Liu, Y., Initiative, Alzheimer's Disease Neuroimaging, 2016. Longitudinal study of impaired Intra- and Inter-Network brain connectivity in subjects at high risk for alzheimer's disease. J. Alzheimers. Dis. 52, 913–927.

Author/s:
Schultz, AP; Buckley, RF; Hampton, OL; Scott, MR; Properzi, MJ; Peña-Gómez, C; Pruzin, JJ; Yang, H-S; Johnson, KA; Sperling, RA; Chhatwal, JP

Title:
Longitudinal degradation of the default/salience network axis in symptomatic individuals with elevated amyloid burden.

Date:
2020

Citation:
Schultz, A. P., Buckley, R. F., Hampton, O. L., Scott, M. R., Properzi, M. J., Peña-Gómez, C., Pruzin, J. J., Yang, H. -S., Johnson, K. A., Sperling, R. A. & Chhatwal, J. P. (2020). Longitudinal degradation of the default/salience network axis in symptomatic individuals with elevated amyloid burden.. Neuroimage Clin, 26, pp.102052-. https://doi.org/10.1016/j.nicl.2019.102052.

Persistent Link:
http://hdl.handle.net/11343/247131

File Description:
published version